/
Article / Book Information

License

Centrifuge model tests on liquefaction-induced settlement and pore water migration in non-homogeneous soil deposits

M. Maharjan and A. Takahashi[*]

Department of Civil Engineering, Tokyo Institute of Technology, 2-12-1 O-okayama, Tokyo 152-8552, Japan

Abstract

This paper presents the results of dynamic centrifuge model tests conducted to investigate the liquefaction mechanism in non-homogeneous soil deposits. Four types of model tests were conducted: one model test involved a uniform soil deposit; one involved continuous layered soil deposit; and two involved discontinuous layered soil deposits. Non-homogeneity in the tests was incorporated by including periodically distributed discontinuous silty sand patches. It was found that more excess pore water pressure (EPWP) remains for a longer period of time in the discontinuous region in non-homogeneous soil deposits compared with the continuous layered and uniform soil deposits. The generation of pore water pressure ceases the supply of a new mass of water after seismic excitation; therefore the dissipation of EPWP becomes the dominant factor for settlement after seismic excitation. The rapid dissipation of EPWP through the discontinuous part in the non-homogeneous soil deposits manifests as a larger settlement in the discontinuous part, causing non-uniform settlements.

Key words: *liquefaction, non-homogeneity, centrifuge model test, excess pore water pressure, non-uniform settlement.*

---

[*]Corresponding author.
Email address: takihiro@cv.titech.ac.jp (A. Takahashi)

1. Introduction

During earthquakes, saturated sandy soils are characterized by a substantial rise in excess pore water pressure (EPWP), leading to dramatic loss of strength and stiffness. When this EPWP reaches a value equal to the initial effective stress, soil particles do not support each other, a phenomenon referred to as zero effective stress condition—a state of initial liquefaction [1-5]. Previous studies that initiated following the observations from liquefaction-related damage during several past devastating earthquakes, have provided significant insights into the liquefaction phenomenon and associated failures. Initially studies were only focused on assessing the triggering factors for liquefaction in clean sandy soils. As the years passed, physical model studies on layered soil deposits evolved. Besides site investigations [6] and numerical analyses [7-9], several experimental studies based on physical model tests, such as one-dimensional column tests [10-13], shaking table tests [10,14], and centrifuge model tests [3,5,15-18], have been conducted to examine the effects of liquefaction in stratified sands. Previous studies indicate that the presence of a relatively impermeable layer (e.g., silt) within a liquefiable sand deposit results in the formation of a water film beneath it because of the trapping of pore water squeezed from the liquefied sand. This plays a key role in the extent of lateral deformations in the sloping surface [10,11,19].

It is noted that the real soil profile is complex and a soil deposit is neither uniform nor consists of continuous layers. Natural sand deposits normally consist of many sublayers with different soil particles and properties, ranging from soft sand lenses to stiff cohesive clay and coarse sand layers. The actual soil profile characterized by various patterns of layering and lensing is very complex, which may have a great effect on geotechnical engineering problems at a site [1]. The recent seismic events of March 11, 2011 in Japan elucidate the further need to understand the complex behavior in a stratified soil profile during liquefaction. However, with the exception of the work by Malvick et al. [18], Ghosh et al. [20], and Chakrabortty and Popescu [21], other physical model tests on liquefaction problems have dealt with uniform clean sand and more recently horizontally layered soil (with uniform properties within distinct soil layers). Malvick et al. [18] conducted a centrifuge test to demonstrate the distribution of pore water during dissipation of earthquake-induced EPWP in a sand slope with continuous embedded silt layers and large postshaking deformations. Ghosh et al. [20] performed a series of centrifuge tests to investigate the effects of localized loose sand in a dense sand deposit subjected to seismic loading. It was found that the presence of loose sand has significant influence on the overall response of the layered strata. Chakrabortty and Popescu [21]

conducted centrifuge tests and numerical simulations on homogeneous and heterogeneous soil deposits consisting of loose pockets of Fraser river sand of relative density 35% surrounded by dense sand of relative density 75%. The results showed that more EPWP is generated in a heterogeneous soil deposit than that in homogeneous soil deposit. Nonetheless, these studies [18,20,21] did not discuss the potential effects of pore water dissipation after shaking on non-uniform settlements as observed in several damage sites during last earthquakes. The conclusions of these studies are not applicable to soil profiles, where the stratification is not only limited to loose and dense sand layers of same material and continuous silt planes. Liquefiable soil deposits consist of thin layers of discontinuous low permeability layers like silt or clay imbedded in sand. To the best knowledge of the authors, numerical or experimental studies related to the presence of discontinuous low permeability layers of silt or clay in liquefiable sand which represents the actual soil profile, have not been carried out. Therefore, the liquefaction potential of a non-homogeneous soil profile is not well understood, though many liquefaction case histories exist.

This paper presents the results of four dynamic centrifuge model tests, conducted to investigate the liquefaction-induced settlement and pore water migration during dissipation of earthquake-induced EPWP in non-homogeneous soil deposits. Two of the model tests were conducted on non-homogenous soil deposits. Non-homogeneity was incorporated by including periodically distributed silty sand patches with a lower permeability than the liquefiable soil specimen. The other two tests were conducted on a uniform soil deposit and a continuous layered soil deposit for comparison purposes. Laminar containers were used in all the tests to properly simulate the boundary conditions. The main objective of the study is to understand the liquefaction mechanism in non-homogenous soil deposits by systematically investigating the effects of non-homogeneity on the amount of EPWP dissipation, drainage path, and settlement.

2. Centrifuge model testing program and conditions

Four dynamic centrifuge model tests were conducted on a 2.45-m-radius Tokyo Tech Mark III centrifuge [22] at a centrifugal acceleration of 40g. The model configurations and the entire test results are presented and discussed in prototype scale units, unless indicated otherwise.

2.1 Soil and pore fluid

Toyoura sand and Silica sand No.8 were used in the tests conducted in this study (Table 1). It is noted that Toyoura sand, also referred to as fine sand, was deposited at a relative density $D_{r1} \approx 50$–55%, and Silica sand No. 8, also referred to as silty sand, was deposited at a relative density $D_{r2} \approx 55$–60%. Silica sand No. 8, being ten times less permeable than Toyoura sand, was employed to create the relatively impermeable layer in layered soil profiles.

The models were saturated with a viscous fluid, i.e., a mixture of water and 2% Metolose (Hydroxypropylmethyl cellulose from Shin-Etsu Chemical Company) by weight of water, to achieve a viscosity of about 40 times the viscosity of water. Previous studies have shown that this type of viscous fluid neither disturbs nor adversely affects the dynamic properties of cohesionless soil [23]. The density and surface tension of this viscous fluid is practically identical to that of water. Also, the viscous fluid simulates the actual prototype permeability of soil.

2.2 Test conditions

The four different model geometries (Models 1–4) of soil thickness 9.8 m with the water table 0.8 m below the surface are depicted in Fig. 1. The model details are presented in Table 2. Model 1 is a homogeneous uniform sand profile, consisting of fine sand only (Fig. 1(a)); Model 2 is a non-homogeneous soil deposit with continuous silty sand layers consisting of three layers of fine sand and two continuous sandwiched silty sand layers of thickness $H_s =$ 1.0 m (Fig. 1(b)); Model 3 and Model 4 are non-homogeneous soil profiles consisting of fine sand layers with two discontinuous silty sand layers of thickness 1.0 m (Fig. 1(c) and (d)). In Model 3, the lower silty sand layer has one 5.0-m-long discontinuous layer of fine sand, i.e., the length is 5.0 m, dividing the silty sand layer into two equal portions of length 7.5 m each, and the upper silty sand layer consists of two discontinuities at the quarter-line of length 2.5 m each (Fig. 1(c)). In Model 4, the lower and upper silty sand layers consist of only one 5.0-m-long discontinuity in each layer at the edge near the left and right boundary, respectively (Fig. 1(d)).

2.3 Model preparation

Models were constructed in a flexible laminar container with dimensions of 500×200×450 mm in length, width, and height, respectively. The box is composed of 20 aluminum alloy rectangular rings separated by linear roller bearings, arranged to permit relative movement between rings with minimal friction. The rings allow the container to move with the soil, which minimizes the side effects, creating a flexible boundary and ensuring the uniform distribution of dynamic shear stresses within the soil.

The models were prepared by air pluviation method, where soil was poured from a constant falling height, using a hopper which was manually moved back and forth along the longest dimension of the box. During the preparation of non-homogeneous soil deposits, Toyoura sand was deposited first with the help of two lightweight blocks placed on both sides (Fig. 2). Then, the remaining parts were filled with Silica sand No. 8 by air pluviation method. Natural soil deposits consist of geological uncertainties with thin seams of less permeable layers (silt and clay) tapered at the end, as a result of successive erosion, transportation, and deposition [24,25]. Therefore, trapezoidal silty sand patches were chosen to model the non-homogeneous soil profile. The soils were first poured such that total model depth is kept to 225 mm in model scale. Then the de-aired Metolose solution was dripped slowly from the top of the container under a vacuum of 760 mmHg until the solution level reached the ground surface. The saturation process for all the tests required approximately 30 hours. After saturation, the sand was again poured by air pluviation method to make the total height equal to 245 mm in model scale, so that the water table was 20 mm below the surface in model scale. It is noted that the soil layers in all the models were leveled and horizontal. Considering the rotational direction, the ground surface has to be curved in the plane parallel to the y-direction in Fig. 1 by 3 mm from the edges of the container. However, since there was no obvious spreading on the ground in the y-direction due to shaking, its effects were neglected.

Accelerometers and pore pressure transducers (PPTs) were installed at the desired locations during model preparation (Table 3) to measure the accelerations and EPWP generated during dynamic loading, respectively. The accelerometers are the piezoelectric type of Sekonic, 111BW with a dimension of 4x12x4 mm and a mass of 2 g. The PPTs are GE Druck miniature model PDCR 81 with a diameter of 6 mm, a height of 12 mm, and a mass of 1.5 g, fitted with a porous element to isolate the fluid pressure. Colored noodles (somen) were placed at the interface between fine sand and silty sand to trace the deformation pattern. Laser displacement transducers (LDTs) and potentiometers were placed on the surface (Table 3) to measure settlements.

2.4 Testing procedure

For the entire centrifuge model tests, the earthquake ground motion recorded at the Hachinohe Port during the 1968 Tokachi-Oki earthquake (NS component) was applied at the base of the model parallel to the long sides of the container (Fig. 3). In Fig. 3, the ground motion applied to the shaker is plotted with a dotted line, and the input motions recorded at the base of the laminar container for each test are plotted with solid lines. As shown in the figure, the waveform simulated by the shaker is not identical to that of the Tokachi-Oki earthquake, but similar in the time domain and agrees fairly well in the frequency domain. Repeatability of applied earthquake motion for all cases was satisfactory.

3. Centrifuge model test results and discussion

3.1. Effect of non-homogeneity on EPWP responses

The EPWP, upon reaching a value equal to the initial vertical effective stress (VES), indicates the occurrence of liquefaction, i.e., a state of initial liquefaction. The EPWP isochrones at the centerline during and after shaking for Models 1 and 2 are shown in Figs. 4 and 5, respectively. Similarly, the EPWP isochrones PPTs located at the centerline and the quarter-line after shaking for Models 3 and 4 are shown in Figs. 6 and 7. Also shown in Figs. 5–7 are the positions of silty sand layers with dashed lines. The EPWP generated rapidly, reaching liquefaction in 13–15 s at all the depths in all the tests. In the case of the uniform homogeneous profile, the EPWP dissipated rapidly in 400 s, shown by changes in EPWP isochrones for PPTs P1, P3, and P5 aligned at the centerline in Fig. 4. In the case of continuous and discontinuous layered soils ,the EPWPs beneath the upper silty sand layer remain equal to the initial effective stress for a longer time even after the cessation of dynamic motion, indicating the trapping of pore water as shown by PPT P7 for Model 2 and PPT P8 for Models 3 and 4 (Figs. 5–7). It can be seen that the EPWPs measured below the upper silty sand layer have nearly the same rate of dissipation after a certain time, which is about 400 s for continuous layered and 300 s for discontinuous layered soils (Figs. 5–7). The faster dissipation in discontinuous layered soils might be due to the presence of discontinuity in the silty sand layer, allowing the pore pressure in the high pore pressure region to easily

find a path to be drained out and transmitted to the low pore pressure region.

When the pore water pressures build up during shaking, dissipation starts mainly towards the ground surface through the shortest possible path [2]. The silty sand layer, being relatively impermeable, hinders the upward movement of pore water. Thus the possible shortest drainage path is the path through P4, P6, P10, and P12 for Models 3 and 4 (see Figs. 1(c) and 1(d)) and finally towards the ground surface. A comparison be1 tween EPWP for PPTs lying along the drainage path (i.e., P6, P10, and P12) and those lying away from the drainage path (i.e., P7, P9, and P11) for Models 3 and 4 is shown in Fig. 8. EPWP is larger for PPTs lying along the drainage path than that for PPTs away from the drainage path, especially at shallow depths (for example at 2.1 m in Fig. 8). The difference in EPWP around the discontinuous region and below the upper silty sand layer creates a hydraulic gradient pointing towards the discontinuous region, which led to the migration of pore water towards the discontinuity region. This concentrates the dissipation of EPWP only through the discontinuity region, increasing the rate and total time of dissipation. As a result, for Models 3 and 4, the EPWP responses at P12, which lies above the discontinuity at 2.1 m depth, are larger than that at P11 above the silty sand layer at the same depth (Figs. 6–8).

The effect of non-homogeneity is illustrated in Fig. 9 by comparing the time histories of EPWP ratios (r_u) for non-homogeneous soil models containing continuous silty sand layers (Model 2) and discontinuous silty sand layers (Models 3 and 4).   The EPWP ratio (r_u) is the ratio of EPWP to the initial vertical effective stress. The pore water remains for a longer period of time beneath and in the silty sand layers in the non-homogeneous soil model containing continuous silty sand layers (P5 and P7 Model 2), compared to that in discontinuous silty sand layers (P6 and P8 for Models 3 and 4). However, the pore water above the discontinuous higher permeability region is larger for models containing discontinuous silty sand layers at shallow depths (P12 for Models 3 and 4). The dissipation of EPWP after shaking at P9 and P10 for Model 2, and that at P11 for Models 3 and 4, which are above the upper silty sand layer, are at about the same rate (Fig. 9). The relatively less permeable layer, acting as a barrier, retards the escape of pore water, resulting the faster rate of dissipation above the upper silty sand layer. The EPWP ratio reduces to half of the initial value (i.e., $r_u = 0.5$) by the first 150 s at P9 and P10 (Model 2) and P11 (Models 3 and 4), but $r_u = 0.9$ at 150 s at P12 for Model 3 and $r_u = 1$ at 150 s at P12 for Model 4.

The effect of distribution of the silica sand pockets was studied for Models 3 and 4. The EPWP response is almost the same for both tests except the response at shallow depth, P12. Nonetheless, as seen in Fig. 9, the value of the EPWP ratio at P12 for Model 4 is nearly equal

to 1 until 200 s, while the value is about 0.8 for Model 3. Moreover, the EPWP ratio is extensively larger until 400 s for Model 4 than that for Model 3. This is due to the effect of length and number of discontinuities in the silty sand layer. Model 4 consists of only one discontinuity in the silty sand layer at the right part of length 5 m in the upper silty sand layer, while Model 3 consists of two discontinuities in the upper silty sand layer of length 2.5 m each. It is evident that the presence of several discontinuities can accelerate the rate of dissipation. The excess pore water can be easily transmitted from the liquefied sand beneath the silty sand layer (high pore pressure region) to the upper sand layer through the highly permeable discontinuities in the silty sand layer (i.e., both drainage layers) due to seepage flow or migration of pore water.

3.2. Effect of non-homogeneity on settlement responses

Settlement time histories at the surface measured by laser displacement transducers (LDTs) and potentiometers for all the tests are presented in Fig. 10. An acrylic base plate was used as a target for LDTs so that they would not sink into the liquefied sand. Similarly, plexiglass was used to support the potentiometers. The potentiometers for Models 1 and 4 malfunctioned; therefore, the records are not presented. Potentiometer S3 indicates a very large noise in settlement time histories (Fig. 10). Displacement at S3 was measured by a contact-type linear position transducer. When the ground settlement is measured using this type of sensor, one end of a rod contacts the ground surface through a plate and the other end of the rod is connected to a sliding contact that forms an adjustable voltage divider in a housing. Since the rod bounces due to the dynamic interaction between the rod and ground surface during shaking, a relatively large noise, i.e., jumps in the record, is observed. However, as seen in Fig. 10, the lower envelope of the record coincides with those obtained using the LDT, i.e., noncontact transducer, in Model 2 in which the uniform settlement is expected. This fact indicates that the lower envelop of the record obtained using the contact-type linear position transducer gives useful information even though it comes with the upward spiky noise.

A significant part of the settlement takes place in all the tests during the initial process of pore pressure build-up, at the time when seismic shaking is applied (up to 70 s). Nonetheless, a part of the settlement during seismic shaking might also be due to compression of dry sand and penetration of target base plates, which was observed during the tests. It is noted that soil settlement is incorporated by the increment in the amount of pore pressure generation and

drainage. The dissipation of EPWP becomes the dominant mechanism after seismic loading as the pore pressure generation ceases the supply of a new mass of water, which is manifested as settlement. Therefore, the settlement induced during dissipation of EPWP after shaking is of great importance for assessing the uneven settlement induced by non-homogeneity of soil deposits and so is further compared in terms of rate of settlement. The variation in rate of settlement for all the models for different time windows is presented in Figs. 11 and 12. In the case of uniform sand and continuous silty sand interlayered soil profiles, the rate of settlement is nearly the same at different locations for different time windows, revealing that the settlement is uniform (see for example S1 and S2, Figs. 11(a) and (b)). In the case of non-homogeneous soil deposits containing discontinuous silty sand layers for Model 3, the rate of settlement is larger at S1 and S2 (which lie above the discontinuity region) than that at S3 (which is above the upper silty sand layer), with few exceptions (Fig. 12(a)). Furthermore, in Model 4 the rate of settlement at S1, which is above the discontinuity part, is extensively larger than at S2, which is above the upper silty sand layer for all time windows (Fig. 12(b)).

The total settlement induced by seepage flow after the shaking at S1, S2, and S3, lying on the ground surface for all models, is presented in Table 4. The settlements at S1, S2, and S3 for Models 1 and 2 indicate uniform settlement. The larger settlements at S1 and S2 for Model 3 and S1 for Model 4 and the smaller settlement at S3 for Model 3 and S2 for Model 4 indicate uneven settlement. Figures 13(a) and (b) indicate the deformation of the noodles imbedded just beneath the upper silty sand layer in Model 3 and just above the upper silty sand layer in Model 4. This was observed during the dissection of the models. Pore water pressure remains larger for a longer period of time in the discontinuous region, causing enough time for the soils to settle. The figures also suggest that more deformation and a larger local settlement occurred in the discontinuous region than in the silty sand layer. These results reveal that the settlement is not uniform in non-homogeneous soil deposits, causing differential settlement of the soil surface.

Figure 14 compares the rate of settlement after shaking at S1 for different time windows. It can be seen that the rate of settlement is presumably greater in Model 1 until 160 s and the rate is larger for Models 3 and 4 after 160 s. EPWP dissipates rapidly within a shorter period of time in Model 1 due to the large value of permeability of Toyoura sand. Consequently, more settlement is induced during a short period of time (70–160 s) in Model 1. The continuous dissipation of EPWP in Models 3 and 4 for a longer period of time causes the rate of settlement to be larger for a longer period of time. Moreover, the rate of settlement for Models 3 and 4 is extensively larger for all the time windows than for Model 2. This results

show a contrast between dissipation of EPWP and rate of settlement (Figs. 9 and 14). The rate of settlement for Model 2 after 200 s remains nearly constant as the EPWP ratio at P10 is also nearly constant until 400 s. In Models 3 and 4, the seepage flow or migration of pore water from the surrounding soil of high pore pressure to discontinuous part for a longer period of time (P12, Fig. 9) causes the rate of settlement to be greater at S1 in Models 3 and 4.   The rate of settlement for Models 3 and 4 is nearly the same until 200 s, while it is substantially larger after 200 s for Model 4 than for Model 3, indicating the larger rate of dissipation of EPWP at P10 in Model 4 (Figs. 9 and 12). This shows that, in Model 4, the EPWP is forced to drain through only one discontinuity layer, increasing the rate and time of dissipation, inducing the larger settlement in the discontinuity region. While in Model 3, the excess pore water is drained out through two discontinuities, reducing the volume of dissipation and inducing the smaller settlement.

4. Summary and conclusions

This study investigated the liquefaction mechanism in non-homogeneous soil deposits by conducting dynamic centrifuge model tests. In particular, two model tests were conducted on non-homogenous soil deposits, where non-homogeneity was incorporated by including periodically distributed discontinuous silty sand patches with lower permeability than the surrounding soil. For comparison purposes, tests were also conducted on a model for continuous layered soil deposit and a model for uniform soil deposit.

This study was focused on modeling the features of actual liquefiable soil profile with discontinuous low permeability layers to properly simulate the generation, redistribution, and dissipation of EPWP during and after shaking. It was found that, in non-homogeneous soil deposits, the pore water was trapped beneath or within less permeable silty sand patches due to the local migration of pore water and difference in permeabilities of the soils, restricting its upward movement. This indicates that the pore water finds a path to drain from the high pore pressure region to the low pressure region, which reveals that the presence of the discontinuous less permeable layer can have substantial effects on the pore pressure dissipation mechanism and drainage. It is determined that the presence of discontinuity of higher permeability in the less permeable soil layer can act as the drainage layer. This concentrates the dissipation of EPWP mainly through the discontinuity region, increasing the rate and total time of dissipation after shaking, inducing the larger settlement in the

discontinuity region. EPWP was accumulated for a longer period of time after shaking in non-homogeneous soil deposits compared with the uniform and continuous layered soil deposits, especially at shallow depths. The settlement induced by seepage at the surface above the discontinuity part was found to be larger than that above the silty sand layer, resulting in non-uniform settlements. The work presented in this study provides new insights into the dissipation of EPWP and the potential causes of non-uniform settlements in actual non-homogeneous soil deposits.

The modeling of liquefaction in the field is complicated due to the various uncertainties in stratigraphic details and geological non-uniformities. It is impossible to model the real soil profile to be exactly the same considering all the geological non-uniformities and taking into account the uncertainties and various soil properties. Attempts have been made to model the multi-layered soil profile consisting of discontinuous thin layers of low permeability based on observations of several damage sites during the last earthquakes to improve the ability to account for them in practice. It is noted that the present study did not give detailed consideration to the degree of saturation of the model ground, boundary effects of the laminar box, and density change due to the application of the seismic motion, which may be improved in future studies.

References

[1] NRC, Liquefaction of soils during earthquakes report, National Academy Press, Washington, DC, 1985.
[2] Ishihara K, Yoshimine M, Evaluation of settlements in sand deposits following liquefaction during earthquakes, Soils and Foundations 1992;32(1):173-88.
[3] Fiegel GL, Kutter BL, Liquefaction mechanism for layered soils, Journal of Geotechnical Engineering 1994;120(4):737-55.
[4] Kramer SL, Geotechnical earthquake engineering, Prentice Hall, 1996.
[5] Brennan A, Madabhushi S, Liquefaction and drainage in stratified soil, Journal of Geotechnical and Geoenvironmental Engineering 2005;131876-85.
[6] Kokusho T, Fujita K, Site investigations for involvement of water films in lateral flow in liquefied ground,

Journal of Geotechnical and Geoenvironmental Engineering 2002;128(11):917-25.

[7] Seid-Karbasi M, Byrne PM, Seismic liquefaction, lateral spreading, and flow slides: a numerical investigation into void redistribution, Canadian Geotechnical Journal 2007;44(7):873-90.

[8] Yoshida N, Finn WDL, Simulation of liquefaction beneath an impermeable surface layer, Soil Dynamics and Earthquake Engineering 2000;19(5):333-38.

[9] Lu XB, Cui P, A study on water film in saturated sand, International Journal of Sediment Research 2010;25(3):221-32.

[10] Kokusho T, Water film in liquefied sand and its effect on lateral spread, Journal of Geotechnical and Geoenvironmental Engineering 1999;125(10):817-26.

[11] Kokusho T, Kojima T, Mechanism for postliquefaction water film generation in layered sand, Journal of Geotechnical and Geoenvironmental Engineering 2002;128(2):129-37.

[12] Scott R, Zuckerman K, Sandblows and Liquefaction in the Great Alaska Earthquake of 1964, Engineering Publication 1606, Washington DC, National Academy of Sciences 1972;170-89.

[13] Tohumcu Özener P, Özaydın K, Berilgen MM, Investigation of liquefaction and pore water pressure development in layered sands, Bulletin of Earthquake Engineering 2008;7(1):199-219.

[14] Liu H, Qiao T, Liquefaction potential of saturated sand deposits underlying foundation of structure, Proceedings of 8th World Conference on Earthquake Engineering 1984; 321-28.

[15] Kulasingam R, Malvick EJ, Boulanger RW, Kutter BL, Strength loss and localization at silt interlayers in slopes of liquefied sand, Journal of Geotechnical and Geoenvironmental Engineering 2004;130(11):1192-202.

[16] Dobry R, Liu L, Centrifuge modeling of soil liquefaction, Tenth World Conference on Earthquake Engineering 1992; 6801-09.

[17] Balakrishnan A, Kutter BL, Settlement, sliding, and liquefaction remediation of layered soil, Journal of Geotechnical and Geoenvironmental Engineering 1999;125(11):968-78.

[18] Malvick EJ, Kutter BL, Boulanger RW, Postshaking shear strain localization in a centrifuge model of a saturated sand slope, Journal of Geotechnical and Geoenvironmental Engineering 2008;134164-74.

[19] Kokusho T, Mechanism for water film generation and lateral flow in liquified sand layer, Soils and Foundations 2000;40(5):99-111.

[20] Ghosh B, Klar A, Madabhushi SPG, Modification of Site Response in Presence of Localised Soft Layer, Journal of Earthquake Engineering 2005;9(6):855-76.

[21] Chakrabortty P, Popescu R, Numerical simulation of centrifuge tests on homogeneous and heterogeneous soil models, Computers and Geotechnics 2012;4195-105.

[22] Takemura J, Kondoh M, Esaki T, Kouda M, Kusakabe O, Centrifuge model tests on double propped wall excavation in soft clay, Soils and Foundations 1999;39(3):75-87.

[23] Okamura M, Abdoun TH, Dobry R, Sharp MK, Taboda VM, Effects of sand permeability and weak aftershocks on earthquake-induced lateral spreading, Soils and Foundations 2001;41(6):63-77.

[24] Atkinson J, The mechanics of soils and foundations, Taylor and Francis, London and New York, 2007.

[25] Kishida H, Damage to reinforced concrete buildings in Niigata City with special reference to foundation engineering, Soils and foundations 1966;6(1):71-88.
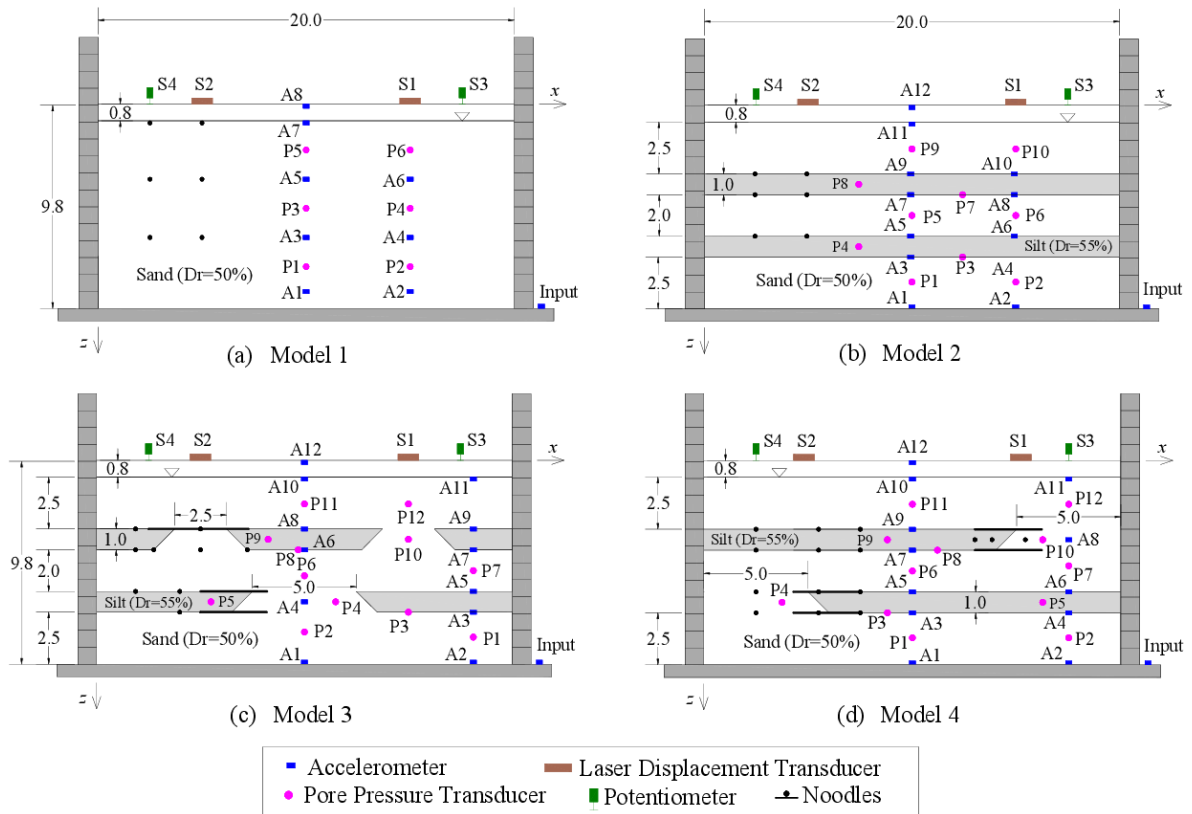
1

2   Fig. 1. Model test configurations. All the units are in meters in the prototype scale
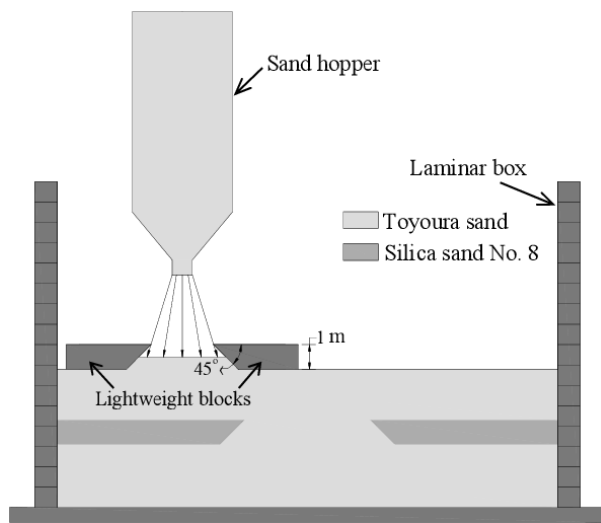

3

4   Fig. 2. Model preparation of non-homogeneous soil deposits.
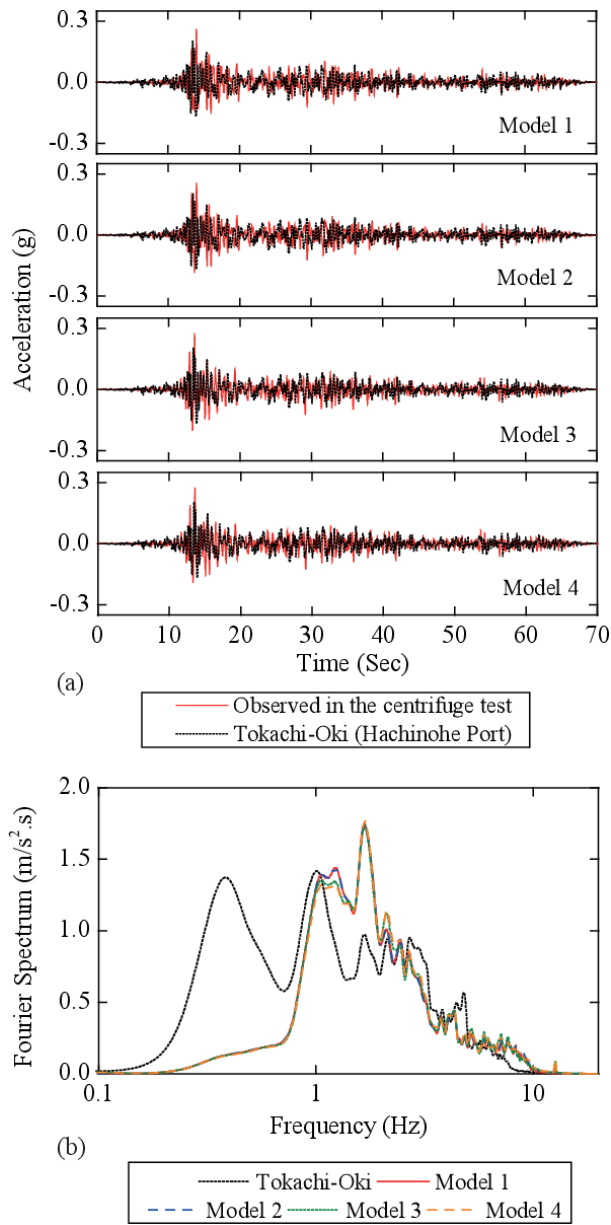
Fig. 3. Acceleration time histories and Fourier spectra of input waves for Hachinohe Port record of 1968 Tokachi-Oki earthquake (NS component).
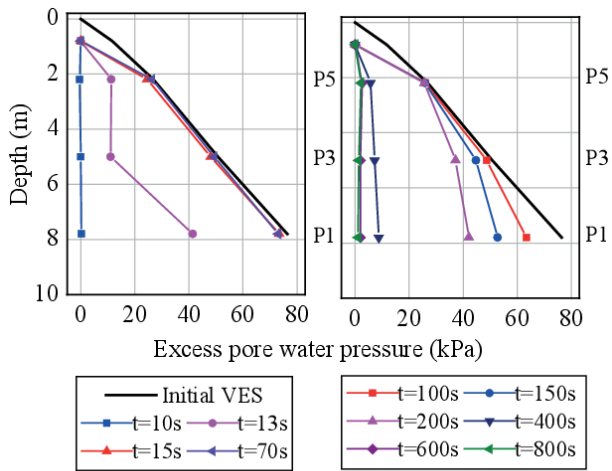
1

(a) During shaking   (b) After shaking

2   Fig. 4. Excess pore water pressure isochrones measured on centerline in Model 1.
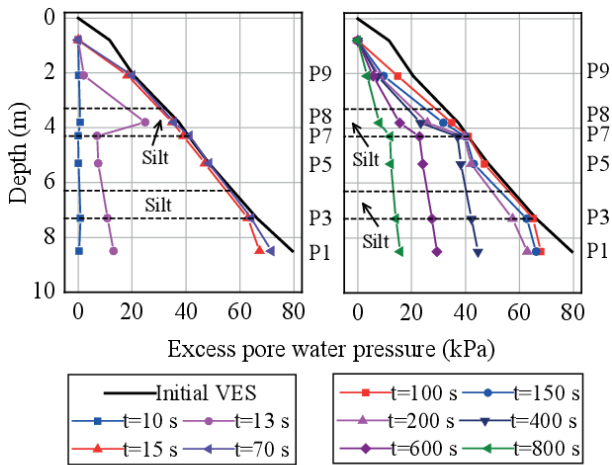
3

(a) During shaking   (b) After shaking

4   Fig. 5. Excess pore water pressure isochrones measured on centerline in Model 2. Dotted lines

5   distinguish the sand and silt layers in the model.

(a) Centerline   (b) Quarter-line
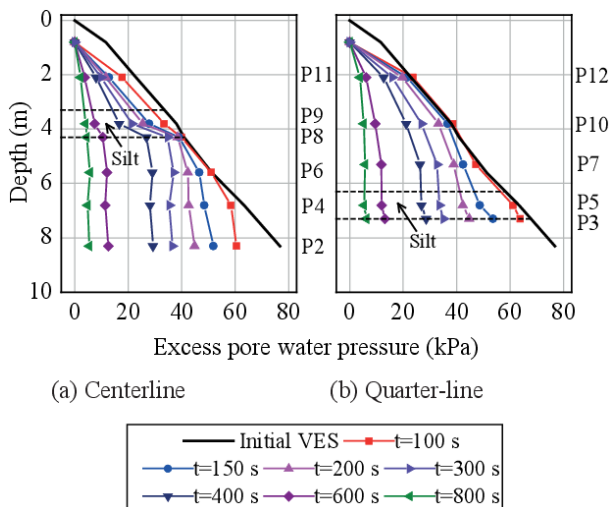
6

7   Fig. 6. Excess pore water pressure isochrones measured in Model 3 after shaking.
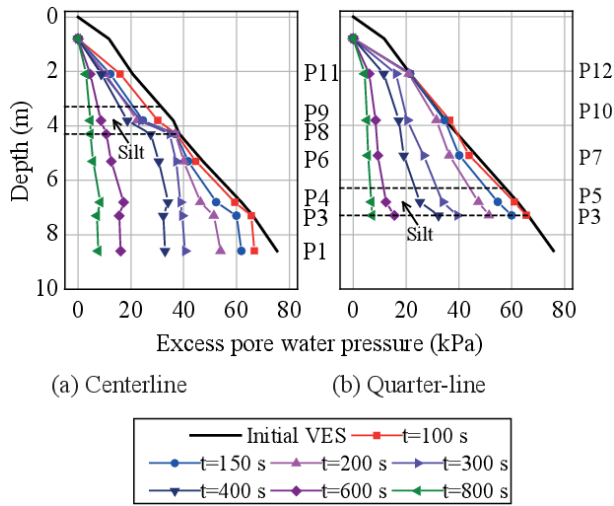
Fig. 7. Excess pore water pressure isochrones measured in Model 4 after shaking.
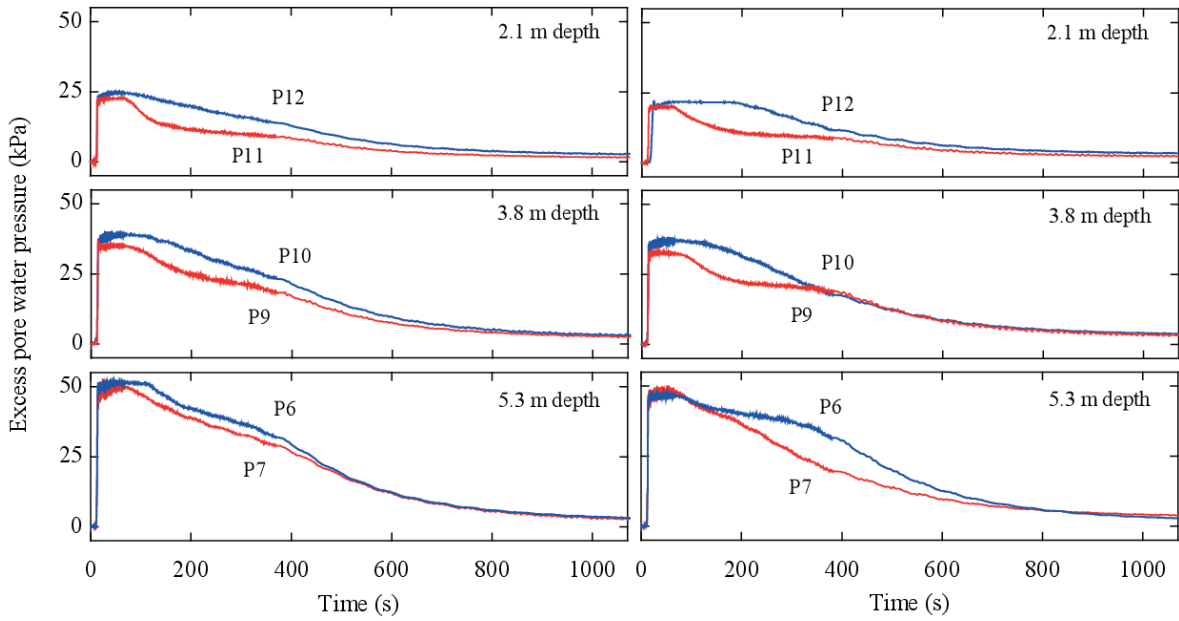
Fig. 8. Excess pore water pressure time histories for Model 3 (left) and Model 4 (right).

16
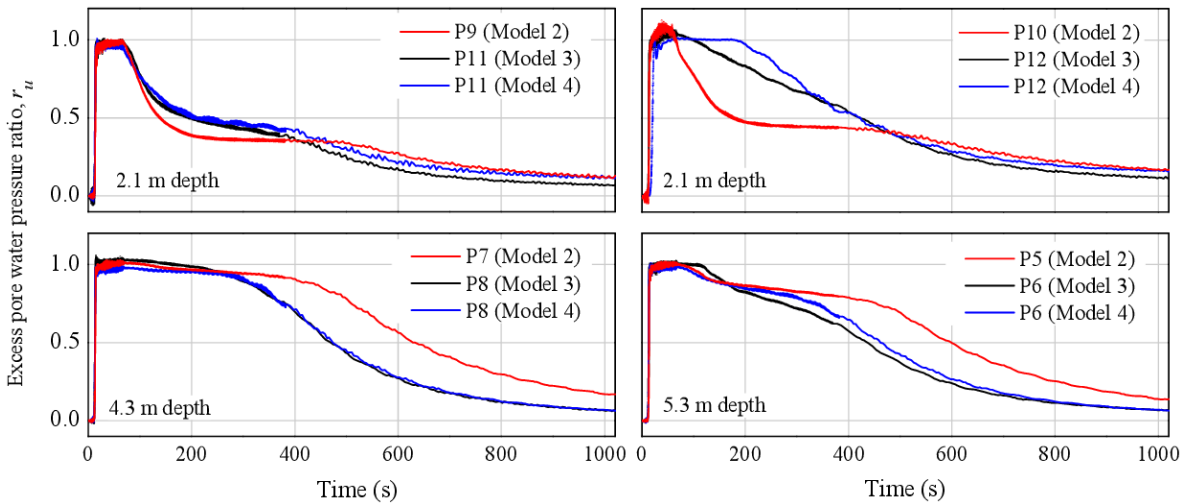
Fig. 9. Time histories of excess pore water pressure ratio (r_u) for Models 2, 3, and 4.
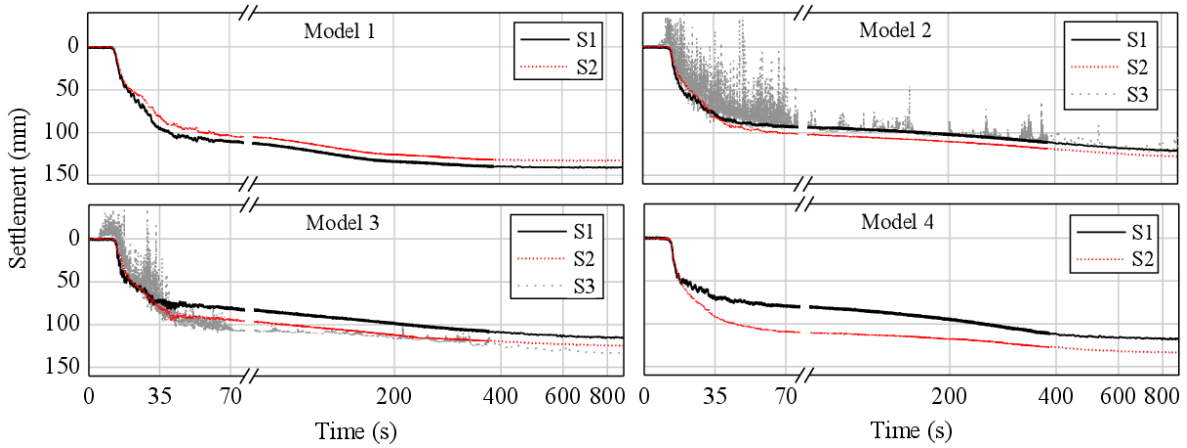
Fig. 10. Settlement time histories for all the model tests.
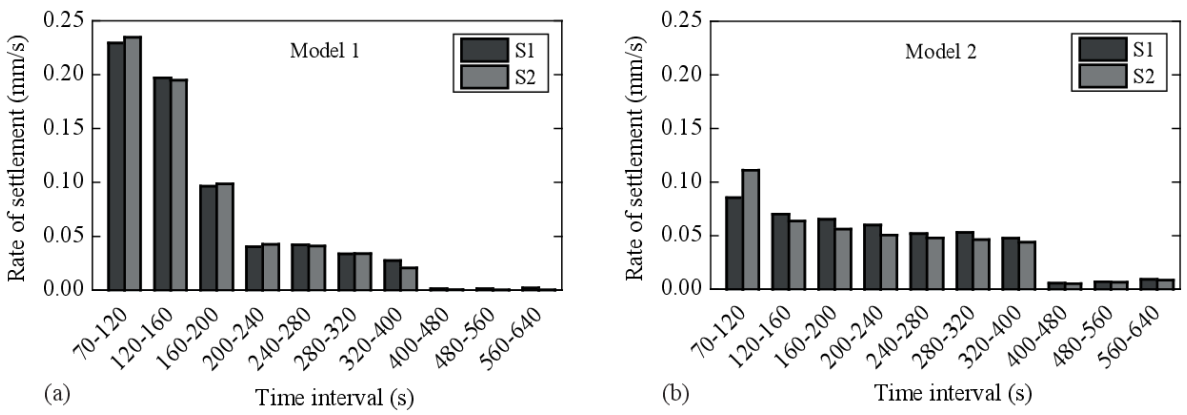
Fig. 11. Variation in rate of settlement: (a) Model 1 and (b) Model 2.
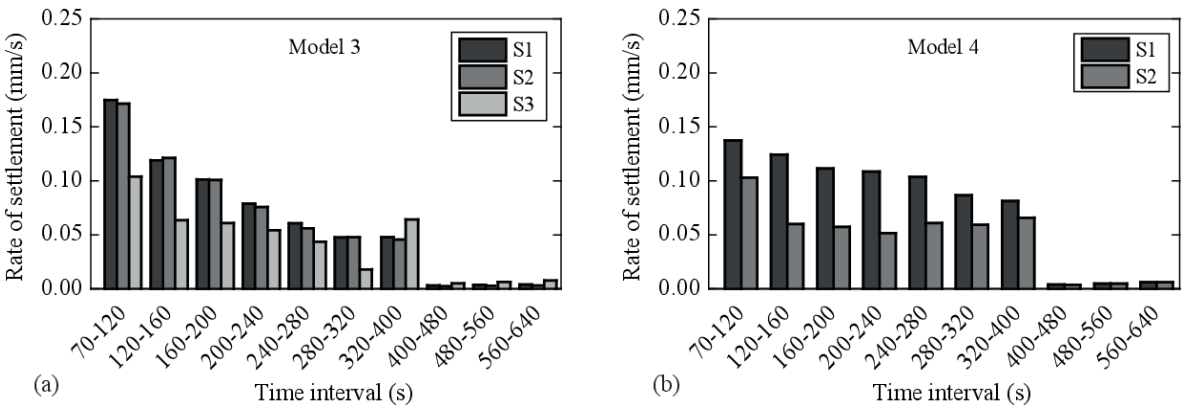
Fig. 12. Variation in rate of settlement: (a) Model 3 and (b) Model 4.
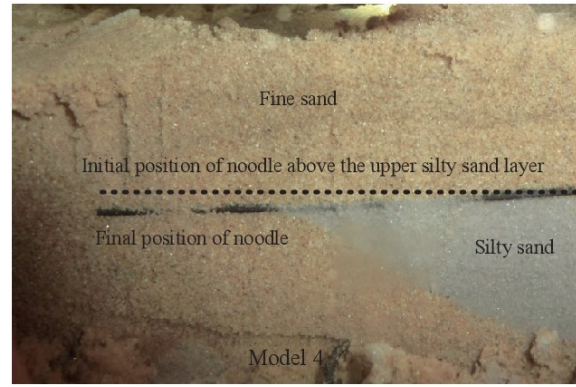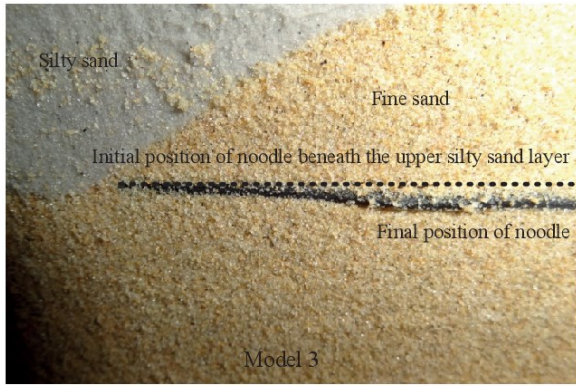
1 (a)   (b)

2 Fig. 13. Settlement pattern at the interface between fine sand and silty sand layers: (a)

3 Beneath the upper silty sand layer in Model 3 and (b) above the upper silty sand layer in

4 Model 4.
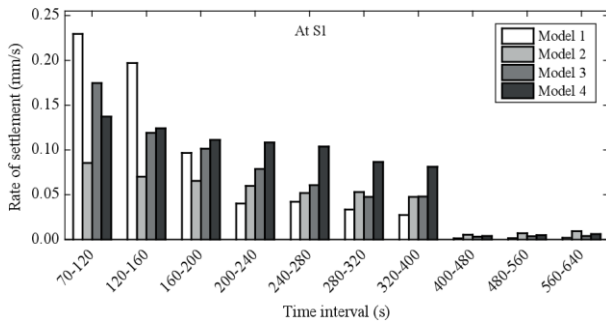
6 Fig. 14. Variation in rate of settlement at S1 for all the model tests.